HHS Public Access

Author manuscript

Nat Struct Mol Biol. Author manuscript; available in PMC 2020 March 05.

Published in final edited form as:

Nat Struct Mol Biol. 2019 September ; 26(9): 808–815. doi:10.1038/s41594-019-0275-1.

Energetics of angstrom-scale conformational changes in an RCK domain of the MthK K^+ channel

John H. Lewis, **Zhe Lu**[1]

Department of Physiology, Perelman School of Medicine, University of Pennsylvania, Philadelphia, PA 19104

Summary

Allosteric proteins transition among different conformational states in a ligand-dependent manner. Upon resolution of a protein's individual states, one can determine the probabilities of these states, thereby dissecting the energetic mechanisms underlying their conformational changes. Here we examine individual RCK domains that form the regulatory module of the Ca^{2+}-activated MthK channel. Each domain adopts multiple conformational states differing on an angstrom scale. The probabilities of these different states of the domain, assessed in different Ca^{2+} concentrations, allowed us to fully determine a six-state model that is minimally required to account for the energetic characteristics of the Ca^{2+}-dependent conformational changes of an RCK domain. From the energetics of this domain we deduced, in the framework of statistical mechanics, an analytic model that quantitatively predicts the experimentally observed Ca^{2+} dependence of the channel's open probability.

Introduction

The Ca^{2+}-activated MthK K^+ channel consists of a transmembrane pore module and a cytoplasmic regulatory module[1]. The regulatory module is formed by eight RCK (regulator of conductance to K^+) domains. Three conformational states, S_1, S_2 and S_3[1, 2] (PDBs 1LNQ, 2FY8 and 4RO0) of the RCK domain have been captured crystallographically (all notations and abbreviations are listed in the Supplementary Note 1). One Ca^{2+}-binding site was initially identified in each RCK domain, and a subsequent study revealed two additional sites[1, 3] (Supplementary Fig. 1). Thus, a total of 24 Ca^{2+}-binding sites are present in the regulatory module. Electrophysiology studies have shown that Ca^{2+} binding to the regulatory module increases the channel's open probability (p_o) by about four orders of magnitude, with a measured Hill coefficient[4] as high as ~20 and an average value of ~10[5, 6]. These behaviors could be explained using a modified version of the Monod-Wyman-

[1]Corresponding author.

Author Contributions

J.H.L and Z.L. designed the study; J.H.L performed experiments, developed analytical tools, and analyzed the data, with the input from Z.L.; J.H.L. and Z.L. interpreted the results and wrote the manuscript.

Competing Interests

There are no competing interests.

Changeux (MWC) model[7], which involves a series of cooperative binding of numerous Ca^{2+} ions[5, 6] (modified MWC models were also used in earlier studies of other types of channels[8, 9]). To a large degree, the apparent strong cooperative Ca^{2+} binding reflects cooperative interactions among RCK domains during channel activation.

To understand the gating mechanism of the MthK channel, it is necessary to examine directly the regulatory module itself, a task that cannot be accomplished with single-channel-current-recording techniques[10, 11]. Here, we use a polarization-microscope-based method[12] to investigate the Ca^{2+}-dependent conformational changes of a single, fluorescently labeled RCK domain within an isolated regulatory module of the MthK channel. Based on the probabilities of individual conformational states determined here, we set out to establish a model that quantitatively accounts for the Ca^{2+}-dependent regulation of RCK's conformational changes, and to obtain, in the framework of statistical mechanics, an analytic solution that can predict the experimentally observed channel's p_o over a wide range of Ca^{2+} concentrations ($[Ca^{2+}]$).

Results

Ca^{2+}-dependent conformational changes in RCK

As described in a companion paper[12], we examined the spatial orientation changes of helix αB in the RCK domain, which is located closest to the channel's gate and adopts a unique orientation in each of the three conformational states identified crystallographically[1, 2]. In one of the eight RCK domains within the regulatory module, this α-helix was labeled with a bifunctional rhodamine molecule via two mutant cysteine residues. Individual labeled regulatory modules (without the pore module) were attached to a coverslip via a four-fold attachment, so that their central axis would be aligned with the optical (z) axis[12]. We collected fluorescence intensities from individual particles via four polarization channels in different Ca^{2+} concentrations (Fig 1a,b), from which we calculated the total emitted intensity (I_{tot}), and inclination (θ) and rotation (φ) angles of the fluorophore's dipole and thus of the α-helix (Fig 1c,d). We also calculated the angle change between two conformations in the actual rotation plane (Ω), which is a function of θ and φ. The state S_2, with an intermediate θ value, was chosen as reference and, consequently, Ω_{22} values were thus distributed around zero. The black traces superimposed on the experimental intensity and calculated angle traces were generated by setting the amplitude of a given event uniformly to the average of the observed values within that event, a procedure that increased the effective signal-to-noise ratio (SNR) and thus angle resolution of individual events. Starting and end points of individual events were statistically determined from the concurrent changes in all four intensity traces.

We identified individual conformational states on a particle-by-particle basis to eliminate the inter-particle variability, and on the basis of both its θ and φ angles, to increase resolution and reliability. As θ is unique for each of the three crystallographically identified conformational states, we used it to identify the corresponding states[12]. To achieve greater accuracy, we estimated the θ value of each state from the distribution of mean θ values of individual particles analyzed separately (Fig. 2a). For each of the three states, the values of either θ or Ω were similar across all examined Ca^{2+} concentrations. Furthermore, across

these concentrations, the mean Θ values of the three states and the mean Ω values among them were comparable to those values predicted from the crystal structures[1, 2] (Fig. 2b).

Ca^{2+} dependence of state probabilities of RCK

We built distributions of the three states in various Ca^{2+} concentrations from the events identified in each Ω trace through particle-by-particle analysis (Fig 3a). From these distributions, we generated the plot of the state probabilities versus the Ca^{2+} concentration (Fig. 3b), showing that all three states were substantially present in the absence or the presence of Ca^{2+}, a defining feature of the MWC model[7]. Consistent with the open-state structure of MthK, in which all RCK domains are in the S_2 state bound with Ca^{2+}, the relative population of S_2 increased with Ca^{2+} concentration, whereas those of S_1 and S_3 decreased (Fig. 3a, b). Thus, RCK can bind Ca^{2+} not only in S_2 but also in S_1 and S_3, although the relative distribution of these states varied with the Ca^{2+} concentration.

The observed Ca^{2+} dependence of RCK conformations strongly implies the existence of minimally six states: three conformations without Ca^{2+} (S_1, S_2 and S_3) and three with n_1 number of Ca^{2+} bound $\left(S_1 \cdot Ca^{2+}_{n_1}, S_2 \cdot Ca^{2+}_{n_1} \text{ and } S_3 \cdot Ca^{2+}_{n_1}\right)$ (Fig. 3c). Given that in the open-state structure[1] all RCK domains adopt S_2, we chose that state as a reference for other states (i), to define the following equilibrium constants:

$$K_{i,2} = \frac{[S_i]}{[S_2]}; \qquad {}^{ca}K_{i,2} = \frac{\left[S_i \cdot Ca^{2+}_{n_1}\right]}{\left[S_2 \cdot Ca^{2+}_{n_1}\right]}; \qquad K_{Di} = \frac{[S_i]\left[Ca^{2+}\right]^{n_1}}{\left[S_i \cdot Ca^{2+}_{n_1}\right]} \quad i = 1, 2, 3 \tag{1}$$

$K_{i,2}$ and ${}^{ca}K_{i,2}$ could be calculated directly from the state populations under zero and saturating Ca^{2+} conditions, respectively, and K_{Di} could be independently determined from the "midpoint" positions of the population curves (Fig. 3b). Together, these constants would fully define the model quantitatively.

The Ca^{2+} dependence of the probability (p_i) of a labeled RCK domain to adopt a given conformation i should reveal its relationship with other RCK domains within the regulatory module. On the one hand, if RCK domains were independent of each other and Ca^{2+} effectively bound to only one site in a RCK domain, the Ca^{2+} dependence of p_i would follow an equation describing the Ca^{2+} and RCK interaction in a one-to-one stoichiometry. On the other hand, if there were a high degree of positive cooperativity among Ca^{2+} sites located within a RCK or among RCK domains, as is the case with the full channel[5, 6], the exponent n_1 of the Ca^{2+}-concentration term in Eq. 1 would be much greater than one.

The observed concentration of RCK in all six conformational states [${}^{obs}S$], i.e., three without and three with n_1 number of Ca^{2+} bound, is given by:

$$\left[{}^{obs}S\right] = [S_1] + [S_2] + [S_3] + \left[S_1 \cdot Ca^{2+}_{n_1}\right] + \left[S_2 \cdot Ca^{2+}_{n_1}\right] + \left[S_3 \cdot Ca^{2+}_{n_1}\right] \tag{2}$$

Under an equilibrium condition, out of the nine equilibrium constants, only five constants (in certain combinations) would be independent parameters in the model (Eq. 1; Fig. 3c). We

chose to use and K_{D2}, $K_{1,2}$, $K_{3,2}$, ${}^{ca}K_{1,2}$ ${}^{ca}K_{3,2}$ in the following expressions. The probability p_i for RCK with and without Ca^{2+} bound is defined by:

$$p_i = \frac{[S_i] + [S_i \cdot Ca_{n_1}^{2+}]}{[{}^{obs}S\ ]} = \frac{K_{i,2} + {}^{ca}K_{i,2}\frac{[Ca^{2+}]^{n_1}}{K_{Di}}}{(K+1) + ({}^{ca}K+1)\frac{[Ca^{2+}]^{n_1}}{K_{Di}}} \quad (3)$$

where K and ${}^{ca}K$ are the ratios of the "decreasing" species (S_1 and S_3) relative to the "increasing" species (S_2) for the cases with and without Ca^{2+} bound, respectively:

$$K = \frac{[S_1] + [S_3]}{[S_2]} = K_{1,2} + K_{3,2};\ {}^{ca}K = \frac{[S_1 \cdot Ca_{n_1}^{2+}] + [S_3 \cdot Ca_{n_1}^{2+}]}{[S_2 \cdot Ca_{n_1}^{2+}]} = {}^{ca}K_{1,2} + {}^{ca}K_{3,2} \quad (4)$$

We fit Eq. 3 globally to the three relations between state probabilities and Ca^{2+} concentrations (Fig. 3b). The resulting values of all equilibrium constants are presented in Supplementary Table 1. The fitted n_1 value was 0.643, consistent with the scenario that Ca^{2+} binding primarily to one site in individual RCK domains promotes the Ca^{2+}-dependent redistribution among the three conformational states. The observed value of less than one may reflect errors of measurements or a modest negative cooperative interaction from another site. In any case, the shallow Ca^{2+} dependence indicates that, in the isolated regulatory module, RCK domains did not exhibit the level of positive cooperativity expected from the steep Ca^{2+} dependence of MthK-channel activation[5, 6], and appeared to undergo the observed conformational changes largely independently.

If individual RCK domains undergo conformational changes independently, then the spontaneous p_o of a MthK channel under a Ca^{2+}-free condition should be related to the probability that individual RCK domains adopt the conformation underlying the channel's open state. The observations that all eight RCK domains adopted S_2 in the open-state structure[1, 3], and that Ca^{2+}, which activates the channel, favored S_2 over other conformations (Fig. 3b) are consistent with the notion that all RCK domains primarily adopt S_2 (dubbed all-S_2) in the open state. Furthermore, the probability of all-S_2 in the absence of Ca^{2+}, given by $p_2^8 = 5.1 \times 10^{-4}$, is comparable to the experimentally determined spontaneous p_o (2.6×10^{-4}) of the MthK channel[6] (Supplementary Table 2).

Deducing an energetic model of the MthK channel

If the RCK domain acts as the basic functional unit of the regulatory module, then establishing an energetic model for the whole MthK channel only requires further deducing the energetics of the gate, plus those of additional unobserved configurations and Ca^{2+}-RCK interactions that occur in the regulatory module of a whole channel. Below, we develop a

model to quantitatively predict the energetic hallmark of regulation of the MthK channel by Ca^{2+}, in the form of the p_0 –[Ca^{2+}] relationship. Detailed statistical mechanics-based derivations are presented in Supplementary Notes 2–4.

In an isolated regulatory module, eight independent RCK domains, each of which can adopt three conformations, giving rise to $3^8 = 6561$ possible permutations. Of those 6561 permutations, if only the all-S_2 species underlies the open state of the regulatory module (RM_o), then the remaining permutations would represent a closed-state configuration (a), denoted by ${}_aRM_c$ (Fig. 4a). As such, individual RCK domains in ${}_aRM_c$ would independently adopt any conformations, with or without Ca^{2+} bound. The concentration of ${}_aRM_c$ would be given by:

$$\left[{}^{obs}_{a}R\ M_c\right] = \left[{}^{obs}S\ \right]^m - \left(\left[S_2\right] + \left[S_2 \cdot Ca^{2+}_{n_1}\right]\right)^m \quad (5)$$

where $[{}^{obs}S]$ is already defined in Eq. 2; and m is 8, the number of the RCK domain.

We also considered a previously proposed configuration (b) of the closed state, denoted by ${}_bRM_c$, where RCK domains would adopt only S_1 or S_3[13]. Thus, in our model, during the transition from ${}_aRM_c$ to ${}_bRM_c$, S_2 would be excluded from all closed species (Fig 4b). The coexistence of Ca^{2+}-free S_1 and S_3 has been observed crystallographically[2]. We further stipulate that ${}_bRM_c$ would exist with or without Ca^{2+} bound[7]. Without explicitly invoking any additional distinct intermediate species, a transition from ${}_aRM_o$ (open state, all RCK domains in S_2) to ${}_bRM_c$(closed state, S_2 excluded) would be perceived as a cooperative transition, because all eight RCK domains must transition to S_1 or S_3. As such, we modeled the binding of Ca^{2+} to individual RCK domains in ${}_bRM$ as being cooperative[4] (Fig. 4b). The concentration of ${}_bRM_c$ should then be expressed as:

$$\left[{}^{obs}_{b}R\ M_c\right] = \left(\left[S_1\right] + \left[S_3\right]\right)^m + \left(\left[S_1 \cdot Ca^{2+}_{n_1}\right] + \left[S_3 \cdot Ca^{2+}_{n_1}\right]\right)^m \quad (6)$$

Regarding the open state, we treated the all-S_2 species alone as the open state (RM_o). The observed concentration of all-S_2 in configuration ${}_aRM$ or ${}_bRM$ (with and without Ca^{2+} bound) would be given by Eq. 7 or Eq. 8.

$$\left[{}^{obs}_{a}R\ M_o\right] = \left(\left[S_2\right] + \left[S_2 \cdot Ca^{2+}_{n_1}\right]\right)^m \quad (7)$$

$$\left[{}^{obs}_{b}R\ M_o\right] = \left[S_2\right]^m + \left[S_2 \cdot Ca^{2+}_{n_1}\right]^m \quad (8)$$

Given that ${}_bRM$ would have far fewer states than ${}_aRM$, it should have higher energy. Implicitly, the binding of Ca^{2+} to at least one additional site (denoted by n_2) in individual RCK domains would be required to lower the free energy of ${}_bRM$. Operationally, Ca^{2+} binding to the n_2 site would regulate the relative distribution between ${}_aRM$ and ${}_bRM$, whereas Ca^{2+} binding to the n_2 site would regulate the relative distribution among the RCK

conformations. However, what is denoted by n_1 may not necessarily be the same physical site in ${}_aRM$ and in ${}_bRM$. Below, we examine first the p_o predicted on the basis of ${}_aRM$ or ${}_bRM$ alone, and then the energetic characteristics of the n_2 site.

Substituting Eqs. 4–8 into the following defining relation:

$$p_o = \frac{[O]}{[O] + [C]} \tag{9}$$

where $[O]$ and $[C]$ denote the concentrations of the open and closed states, we obtained the expressions for the regulatory module's p_o in ${}_aRM$ and ${}_bRM$:

$${}^{obs}_{a}p_{o} = \frac{\left[{}^{obs}_{a}R\ M_o\right]}{\left[{}^{obs}_{a}R\ M_c\right] + \left[{}^{obs}_{a}R\ M_o\right]} = \frac{\left(1 + \frac{\left[Ca^{2+}\right]^{n_1}}{K_{D2}}\right)^m}{\left(K + 1 + \left({}^{ca}K + 1\right)\frac{\left[Ca^{2+}\right]^{n_1}}{K_{D2}}\right)^m} \tag{10}$$

$${}^{obs}_{b}p_{o} = \frac{\left[{}^{obs}_{b}R\ M_o\right]}{\left[{}^{obs}_{b}R\ M_c\right] + \left[{}^{obs}_{b}R\ M_o\right]} = \frac{1 + \left(\frac{\left[Ca^{2+}\right]^{n_1}}{K_{D2}}\right)^m}{1 + \left(\frac{\left[Ca^{2+}\right]^{n_1}}{K_{D2}}\right)^m + K^m + \left({}^{ca}K\frac{\left[Ca^{2+}\right]^{n_1}}{K_{D2}}\right)^m} \tag{11}$$

The p_o-$[Ca^{2+}]$ curves calculated with Eqs. 10 and 11 (Fig. 4c) exhibited the following features (all parameters in this paragraph are tabulated in Supplementary Table 2). First, the predicted EC_{50} value of 1.6 mM for ${}_aRM$ is comparable to the 0.97 mM value estimated from the fit of a version of the Hill-equation[4] (Eq. 58, Supplementary Note 4) to a previously observed channel's p_o–$[Ca^{2+}]$ relationship[6]. Second, as already mentioned above, the predicted minimal ${}_ap_o$ of ${}_aRM$ is close to the observed channel's minimal p_o in the absence of Ca^{2+} (${}_{ch}p_o$). Third, the predicted maximal ${}^{ca}_{b}p_{o}$ of ${}_bRM$ is 0.98, which is the same as the observed channel's maximal $p_o({}^{ca}_{ch}p_{o})$ of 0.98.[6] Finally, the end point of the curve for ${}_aRM$ practically matches the starting point of the curve for ${}_bRM$. Thus, combining Eqs. 10 and 11, which underlie the two curves in Fig. 4c, would adequately account for the full range of the observed p_o of the channel $\left({}^{obs}_{ch}p_{o}\right)$.

A channel model that contains configurations *a* and *b* is shown in Figure 5a. In configuration *a*, Ca^{2+} binding to all sites n_1 in a regulatory module leads to ${}_aRM \cdot \left(Ca^{2+}_{n_1}\right)_m$, whereas in configuration *b*, Ca^{2+} binding to all sites n_2 in a regulatory module leads to ${}_bRM \cdot \left(Ca^{2+}_{n_2}\right)_m$.

In all three RCK conformations, Ca^{2+} would bind to site n_2 with the same unknown K_D (dubbed K_{Dn2}), but it would bind to site n_1 with three different K_{Di} values, all of which were properly scaled and expressed in the form of K_{D2} in the above equations. Equalizing the average free energy of ${}_{a}RM \cdot \left(Ca^{2+}_{n_1}\right)_m$ and that of ${}_{b}RM \cdot \left(Ca^{2+}_{n_2}\right)_m$ requires that the overall apparent K_D for Ca^{2+} binding to site n_1 (K_{Dn1}) be the same as K_{Dn2}. Thus, we could deduce the value of K_{Dn2} from that of K_{Dn1} in accordance with the relation (Supplementary Note 4):

$$K_{Dn2} = K_{Dn1} = \frac{K+1}{{}^{ca}K+1} K_{D2} \tag{12}$$

which yields 0.38 mM. With an explicit inclusion of the n_2 site, the total open species in ${}_{a}RM$ and ${}_{b}RM$ (RM_o, Eqs. 5 and 6) and the total closed species(RM_c, Eqs. 7 and 8) would be defined as:

$$\left[{}^{obs}_{ch}R\ M_o\right] = \left[{}^{obs}_{a}R\ M_o\right] + \left[{}^{obs}_{b}R\ M_o \cdot \left(Ca^{2+}_{n_2}\right)_m\right] \tag{13}$$

$$\left[{}^{obs}_{ch}R\ M_c\right] = \left[{}^{obs}_{a}R\ M_c\right] + \left[{}^{obs}_{b}R\ M_c \cdot \left(Ca^{2+}_{n_2}\right)_m\right] \tag{14}$$

Substituting Eqs. 13 and 14 (in the form of energetic constants) into Eq. 9 yielded the p_o–$[Ca^{2+}]$ relation for the whole channel:

$$\begin{aligned} {}^{obs}_{ch}p_{\ o} = {} & \left(1+\frac{\left[Ca^{2+}\right]^{n_1}}{K_{D2}}\right)^m + \left(\frac{\left[Ca^{2+}\right]^{n_2}}{K_{Dn2}}\right)^m \left(1+\left(\frac{\left[Ca^{2+}\right]^{n_1}}{K_{D2}}\right)^m\right)\left(1+\frac{\left[Ca^{2+}\right]^{n_1}}{K_{D2}}\right)^m \\ & \left(1-{}_{g}K\right) + \left(\frac{\left[Ca^{2+}\right]^{n_2}}{K_{Dn2}}\right)^m \left(1+\left(\frac{\left[Ca^{2+}\right]^{n_1}}{K_{D2}}\right)^m\right) \\ & + \left(\left(K+1+({}^{ca}K+1)\frac{\left[Ca^{2+}\right]^{n_1}}{K_{D2}}\right)^m + \left(\frac{\left[Ca^{2+}\right]^{n_2}}{K_{Dn2}}\right)^m \left(K^m + \left({}^{ca}K\frac{\left[Ca^{2+}\right]^{n_1}}{K_{D2}}\right)^m\right)\right){}_{g}K \end{aligned} \tag{15}$$

where ${}_{g}K$ is the apparent equilibrium constant of the gate, as defined in Supplementary Note 4; K describes the relative distribution between "$[S_1] + [S_3]$" (unbound closed species in configuration *b*) and $[S_2]$(open species); and ${}^{ca}K$ describes the relative distribution between the corresponding Ca^{2+}-bound closed and open species (Eq. 4). In an ideal case where the total amount of energy related to this fully reversible conformation redistribution equals that derived from Ca^{2+} binding, K^m should equal to ${}^{ca}K^{-m}$. We noted that fitted K (1.576) is slightly smaller than ${}^{ca}K^{-1}$ (1.686)(Supplementary Table 1). The small "excess" Ca^{2+}-binding energy defined by $kT\ln\left(K^{ca}K^{-1}\right)^{\frac{m}{2}}$ could, in principle, help to energetically equalize the open and closed states of the channel gate itself. $\left(K^{ca}K^{-1}\right)^{\frac{m}{2}}$ yields a value of 1.3; within

experimental errors, a $_gK$ of 1.3 (slightly favoring the closed state) would be sufficient to close the small gap between the observed minimal p_o and that predicted by the model for the regulatory module alone (i.e., Eq. 15 where $_gK$ is set to 1).

To test the predictability of our model, we calculated a p_o−[Ca^{2+}] curve with Eq. 15, using the parameters determined from fluorescence polarization measurements (Fig. 3c; Supplementary Table 1; $_gK$ = 1.3, K_{Dn2} = 0.38 mM, and n_2= 1). The calculated curve matches the p_o−[Ca^{2+}] relationship previously determined by electrophysiology[6], within the experimental errors (Fig. 5b, data points colored light blue and the curve colored orange). It is noteworthy that when explicitly expressed, Eq. 15 would be fully defined by a total of ten parameters: $K_{1,2}$, $K_{3,2}$ (expressed together as K), $^{ca}K_{1,2}$ and $^{ca}K_{3,2}$ (expressed as ^{ca}K), n_1 and K_{D2}, all determined from studying RCK; m determined by crystallography; n_2, K_{Dn2} and $_gK$ can be deduced as described above. This large number of parameters cannot be extracted by fitting the p_o−[Ca^{2+}] curve with a Hill equation[4].

For comparison, we estimated $_gK$ and K_{Dn2} by fully constraining them with experimental measurements. First, we used Eq. 59 (Supplementary Note 4) to directly calculate $_gK$ from the constant K (Eq. 4; Supplementary Table 1) and minimal $_{ch}p_o$ of the channel (Supplementary Table 2; reference[6]), obtaining a slightly larger value of 1.7. We then determined K_{Dn2} through a global fit of Eq. 15 to the experimental p_o−[Ca^{2+}] relationship of the channel[6] (Fig. 5b, blue curve) and the three plots regarding Ca^{2+}-dependence of RCK conformations in the isolated regulatory module (Fig. 3b, black curves; all resulting parameters are tabulated in Supplementary Table 1). The fit yielded a K_{Dn2} value of 0.39 mM, nearly the same as the deduced 0.38 mM. In the fit, $_gK$ was set at 1.7, instead of 1.3 and, consequently, the calculated (orange) and fitted (blue) curves diverged slightly and can be recognized. The inferences are that given the rather small $_gK$, the observed channel's operational energy primarily reflects that of the regulatory module, and that the present model (Eq. 15; Fig. 5) quantitatively predicts the experimental MthK's p_o−[Ca^{2+}] relationship.

Discussion

The regulatory module of the MthK channel harvests the so-called gating energy from the binding of Ca^{2+} to its eight RCK domains. In the model described here, each RCK in $_aRM$ may independently adopt three conformations, with or without Ca^{2+} bound. Even considering only a single Ca^{2+} site per RCK, eight independent RCK domains could generate 6^8 (~1.7 million) possible permutations or 3^8 (6561) in the absence of Ca^{2+}. If among this large number of permutations, only all-S_2 is associated with the open conformation of the channel, the spontaneous p_o would be primarily determined by entropic energy, given the vastly different numbers of the accessible open versus closed species. The large number of closed species should be depopulated toward the limiting case of effectively one state by Ca^{2+} binding, and the collective probability of all closed species in saturating Ca^{2+} concentrations should be much smaller than the probability of the open species, such that the channel's p_o would rise from the minimum towards 1. Indeed, electrophysiology studies have shown that Ca^{2+} regulation of the MthK channel occurs primarily while the gate is closed[5, 6].

A proposal that a MthK channel can open from the all-S_1 state has been put forward, on the basis of the following observations[13]. First, an all-S_1 form of the isolated regulatory module was captured crystallographically, with Ba^{2+} present at multiple sites within individual RCK domains. Second, Ba^{2+} can activate the MthK channel, albeit with lower efficacy and potency than Ca^{2+}. Third, a mutation at a putative Ba^{2+} binding site eliminates the ability of Ba^{2+} to activate the channel. Thus far, there is no structural evidence to link all-S_1 to the open state of the channel yet. In any case, the probability of all-S_1 species predicted from our measurements is low, and thus the p_o–$[Ca^{2+}]$ curves calculated from two compared models, in which either only all-S_2 or all-S_2 and all-S_1 are open species, are visually indistinguishable, even on double logarithmic plots (Supplementary Fig. 2). Should Ba^{2+} act differently than Ca^{2+}, such that Ba^{2+} binding to RCK would populate S_1 instead of S_2, modeling all-S_1 species as an open state could in principle accommodate the observed channel activation by Ba^{2+}. Here we considered only all-S_2 as the open species for the following reasons. First, only all-S_2 was observed in an open-state structure of the MthK channel. Second, we intended to account for the Ca^{2+}-dependent regulation, for which all-S_2 being the open species is sufficient. Third, we do not have the quantitative information regarding Ba^{2+}-bound RCK to express the all-S_1 species in the analytic model. In any case, the present model could be expanded to include additional open and closed species to account for other features of the channel.

As mentioned, one defining feature of the MWC model is that a protein may adopt one of two (or more) alternative states (R or T) with or without ligand bound[7]. A second defining feature is that all protomers in the protein must be in the same state. In our model, ~1.7 million species form a grand canonical ensemble in terms of statistical mechanics, and given its thermodynamic nature, the model does not concern the paths between any pair of states, regardless of whether they exist in the same or between coexisting configurations *a* and *b* (here divided merely for a conceptual purpose). In the vast majority of closed states of either configuration, RCK domains in different conformations coexist. Thus, our model does not satisfy that the second defining feature of the MWC model.

As a special case of the MWC model, the Hill equation[4] would be defined here by minimal and maximal P_o, EC_{50} and the Hill coefficient (Eq. 58, Supplementary Note 4). In our model, the minimal or maximal P_o each is defined by three parameters $\left(\left[\left(K_{1,2}+K_{3,2}+1\right)^m\ {}_gK\right]^{-1}\ \text{or}\left[\left({}^{ca}K_{1,2}+{}^{ca}K_{3,2}\right)^m\ {}_gK\right]^{-1}\right)$. The EC_{50} depends on all independent parameters in a complex manner, and the analytic expression of the Hill coefficient would be even more complex, if it is reachable. Thus, extracting four parameters from the p_o–$[Ca^{2+}]$ relationship of the MthK channel using the Hill equation could lead to an empirical quantitative description of observed Ca^{2+}-dependent redistribution between the total open species and the total closed species, but would not reveal the energetic mechanism underlying Ca^{2+}-dependent gating conformational changes that occur in the regulatory module.

Thus, examining the behaviors of individual RCK domains is necessary to understand the energetic mechanism of the MthK channel. The channel model deduced here on the basis of energetics of the RCK domain well predicts the observed p_o–$[Ca^{2+}]$ relationship[6], in which

the binding of Ca^{2+} increases the channel's p_o by two distinct mechanisms. First, independent, non-cooperative binding of Ca^{2+} to individual RCK domains populates S_2 over S_1 or S_3, enhancing the probability of individual RCKs to adopt S_2 and thereby fine tuning p_o. Second, cooperative Ca^{2+} binding would populate ${}_bRM$ over ${}_aRM$, of which the former has fewer closed states. These tuning and configuration-switching mechanisms primarily underlie the shallow and steep phases of the p_o–$[Ca^{2+}]$ relationship, respectively. The good agreement between our data obtained with the isolated regulatory module and previous electrophysiology data with the whole channel validates our approach. The present energetic study serves as a foundation for a subsequent study[14], where we use the present method to examine the multi-state conformational dynamics of RCK, and demonstrate how the resulting dynamic information can be used as a temporal template to link its existing structures.

Online Methods

Sample preparation and data recording

As described in reference[12], a recombinant protein of the MthK channel's regulatory module, which contained a N-terminal recognition sequence for biotin ligase, a C-terminal His-tag with a preceding specific-protease-cutting sequence, and the double E146C and L153C mutation in helix αB, was produced using the bacterial BL-21 expression system. The protein was labeled with bifunctional rhodamine (Bis-((N-Iodoacetyl)-Piperazinyl)-Sulfonerhodamine; Invitrogen B10621) via the two mutant cysteine residues and attached to a coverslip conjugated with streptavidin (Arrayit) via biotinylated N-termini. Polarized emissions from individual bi-functional rhodamine labels, excited in the evanescent field created at the surface of the sample coverslip by circularly polarized laser beam (532 nm), were collected via a fluorescence microscope with four polarization emission channels onto an electron-multiplying charge-coupled device camera, while the sample protein was immersed in a solution containing 200 mM KCl, Ca^{2+} of various concentrations, and 10 mM HEPES titrated to pH 8.0, where 1 mM EGTA was used as a buffer in the nominal Ca^{2+}-free and low (0.1 mM) Ca^{2+} solutions.

Data analysis

Also as described in reference[12], each intensity of the four emission components collected from a given fluorophore was a direct summation of individual pixels. I_{tot}, θ, φ, and Ω were calculated using Eqs. 62, 63, 61, and 70 in the Supplementary Note 3 and 6 in the above reference, respectively. Conformational transitions and states were identified in two separate steps. A *changepoint* algorithm was applied to the intensity traces to detect the transitions between conformational events, whereas a *k*-means-cluster-based algorithm was applied to identify the conformational states of individual events based on both θ and φ.

Data availability

Data and materials described here will be made available upon reasonable request.

Supplementary Material

Refer to Web version on PubMed Central for supplementary material.

Acknowledgments

We thank Y. Zhou for technical support; Y. Jiang and R. MacKinnon for providing the cDNA of MthK; V. Pau and B. Rothberg for sharing their published data for comparison; and P. De Weer, T. Hoshi, and B. Salzberg for critiques of our manuscript at different stages of its development. This study was supported by the grant GM055560 from the National Institute of General Medical Sciences of the National Institutes of Health to Z.L.

References

1. Jiang Y et al. Crystal structure and mechanism of a calcium-gated potassium channel. Nature 417, 515–522 (2002). [PubMed: 12037559]
2. Ye S, Li Y, Chen L, & Jiang Y Crystal structures of a ligand-free MthK gating ring: insights into the ligand gating mechanism of K^+ channels. Cell 126, 1161–1173 (2006). [PubMed: 16990139]
3. Pau VP et al. Structure and function of multiple Ca^{2+}-binding sites in a K^+ channel regulator of K^+ conductance (RCK) domain. Proc. Natl. Acad. Sci. U. S. A 108, 17684–17689 (2011). [PubMed: 21997217]
4. Hill AV The possible effects of the aggregation of the molcules of hemoglobin on its dissociation cruves. The Journal of Physiology XL, iv–vii (1910).
5. Zadek B & Nimigean CM Calcium-dependent gating of MthK, a prokaryotic potassium channel. J. Gen. Physiol 127, 673–685 (2006). [PubMed: 16735753]
6. Pau VP, Barca-Heidemann K, & Rothberg BS Allosteric mechanism of Ca^{2+} activation and H^+-inhibited gating of the MthK K^+ channel. J. Gen. Physiol 135, 509–526 (2010). [PubMed: 20421375]
7. Monod J, Wyman J, & Changeux JP On the nature of allosteric transitions: a plausible model. J. Mol. Biol 12, 88–118 (1965). [PubMed: 14343300]
8. Marks TN & Jones SW Calcium currents in the A7r5 smooth muscle-derived cell line. An allosteric model for calcium channel activation and dihydropyridine agonist action. J. Gen. Physiol 99, 367–390 (1992). [PubMed: 1316936]
9. Zagotta WN, Hoshi T, & Aldrich RW Shaker potassium channel gating. III: Evaluation of kinetic models for activation. J Gen. Physiol 103, 321–362 (1994). [PubMed: 8189208]
10. Sakmann B & Neher E Single-Channel Recording (Plenum Press,1995).
11. Miller C Ion channel reconstitution (Plenum, New York, 1986).
12. Lewis JH & Lu Z Resolving angstrom-scale protein-conformational changes by analyzing fluorescence anisotropy. Nat. Struct. Mol. Biol 26, 802–807 (2019). [PubMed: 31488909]
13. Smith FJ, Pau VP, Cingolani G, & Rothberg BS Crystal structure of a Ba^{2+}-bound gating ring reveals elementary steps in RCK domain activation. Structure 20, 2038–2047 (2012). [PubMed: 23085076]
14. Lewis JH & Lu Z Integrating spatiotemporal features of a ligand-regulated, multi-state allosteric protein. Nat. Struct. Mol. Biol 26, 816–822 (2019). [PubMed: 31488908]

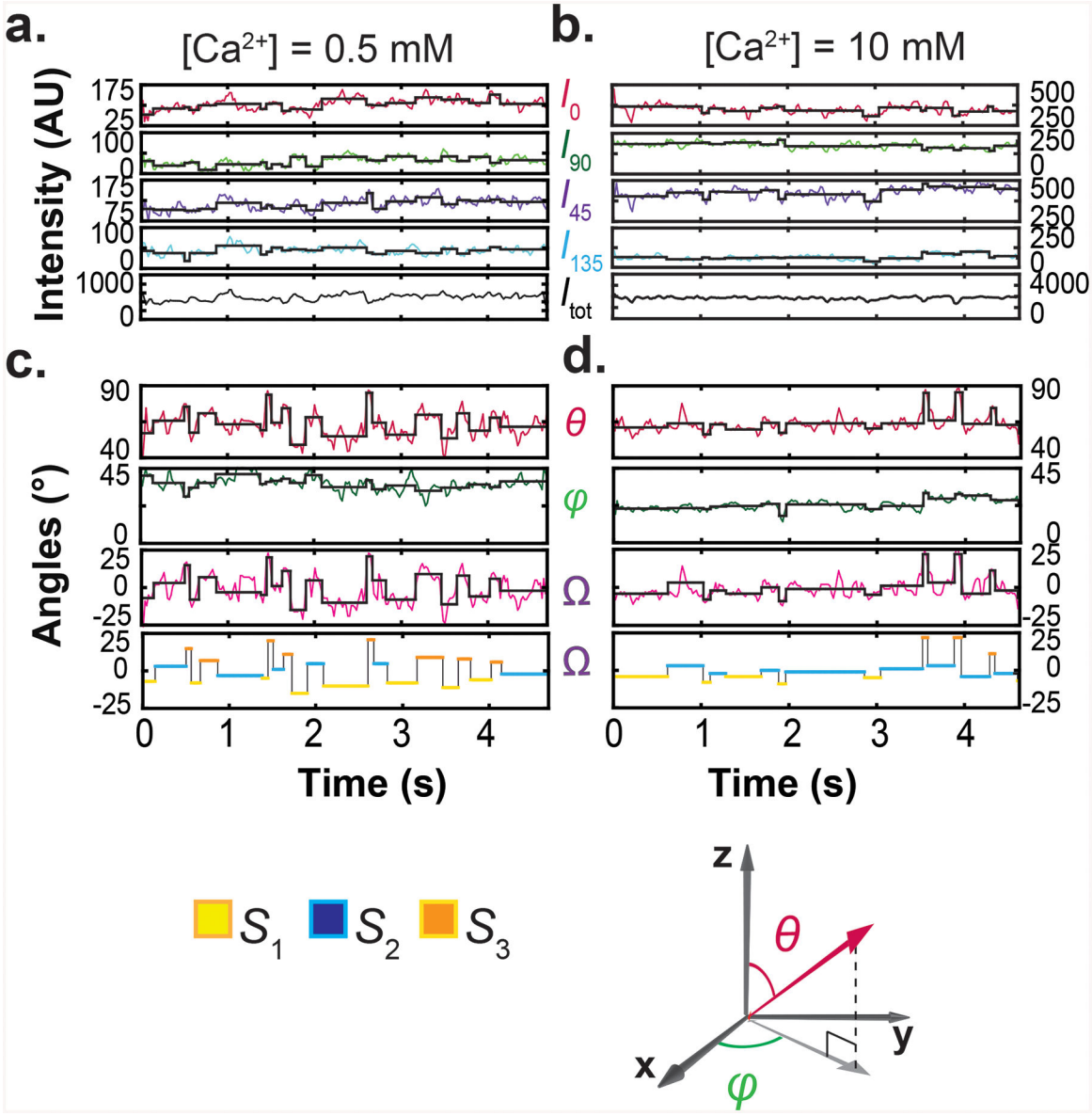

Figure 1.

Polarized-fluorescence intensities and calculated I_{tot}, θ, φ and Ω at two Ca^{2+} concentrations. **a, b.** Four intensity components (I_0, I_{45}, I_{90} and I_{135}) of single particles recorded over ~5 seconds in 0.5 mM (**a**) and 10 mM (**b**) Ca^{2+}, and I_{tot} calculated from I_0, I_{45}, I_{90} and I_{135}. **c, d.** Values of θ and φ calculated from the four intensity components and values of Ω calculated relative to S_2. Transition points of the black traces superimposed on the experimental intensity and angle traces were determined by a *changepoint* analysis whereas the constant values between the transitioning points are means of the observed data. For easy visualization, a colored-for-conformational-state version of the black trace for Ω is shown below. For reference, coordinate systems are shown at the lower right corner.

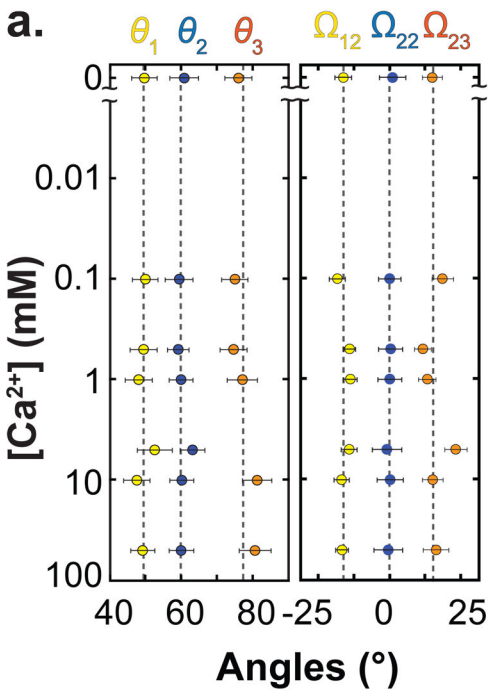

b.

	θ_1	θ_2	θ_3
Crystallography	52°	62°	70°
Polarization	49°±4°	60°±3°	76°±4°

	Ω_{12}	Ω_{22}	Ω_{23}
Crystallography	12°	0°	10°
Polarization	13°±3°	0.2°±2°	12°±4°

Figure 2.

Comparison of θ and Ω angles determined from single-molecule fluorescence polarization measurements with those from existing crystal structures. **a.** θ and Ω values (mean ± σ; n = 110–1589) of the labeled helix in the three conformational states, determined over a range of Ca^{2+} concentrations in the fluorescence study and analyzed on a particle-by-particle basis. **b.** θ and Ω values deduced from the three crystal structural states[1, 2] compared with mean θ and Ω values determined from fluorescence measurements. These mean values and their associated σ values of θ and Ω are calculated from their respective arithmetic means of individual analyzed particles, examined over the entire Ca^{2+} range shown in **a**.

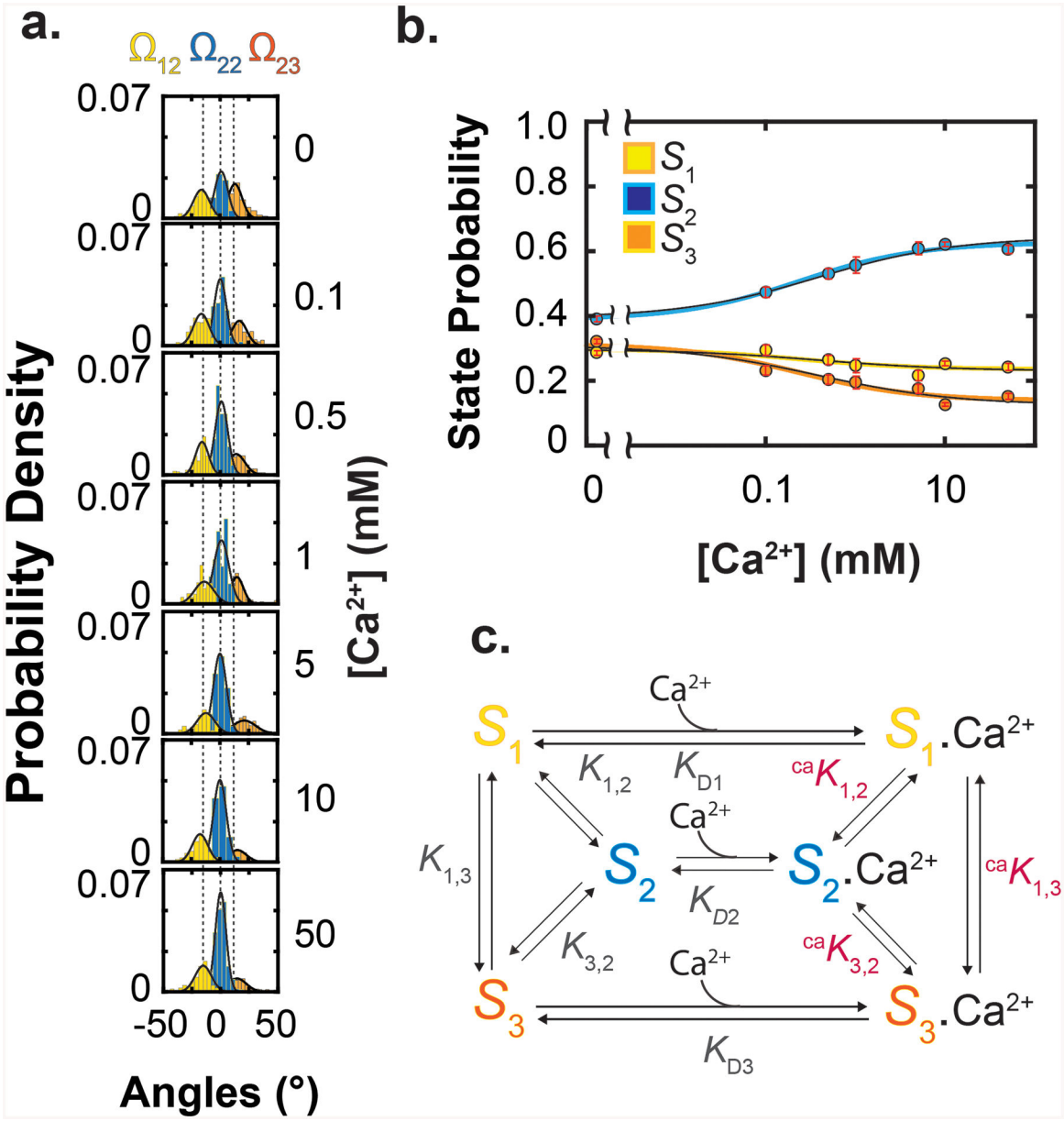

Figure 3.

Ca^{2+} dependence of state probabilities and state diagram of an energetic model of RCK. **a**. Distributions of Ω angle values at various Ca^{2+} concentrations obtained from total 980 particles. For illustration, the curves were calculated from the values of the mean and standard deviation σ. **b**. Probabilities (mean ± s.e.m.; n = 110 – 1589) of a RCK to adopt the three conformational states, calculated from the data shown in **a** and plotted against Ca^{2+} concentrations. The state-color-coded curves superimposed on the data correspond to a global fit of Eq. 3 to the three plots in Fig. 3b alone, whereas the thin black curves correspond to a global fit of Eq. 15 to all of the plots in Fig. 3b and Fig, 5b together. **c**. A six-state model of RCK where it exists in three conformations with or without Ca^{2+} bound.

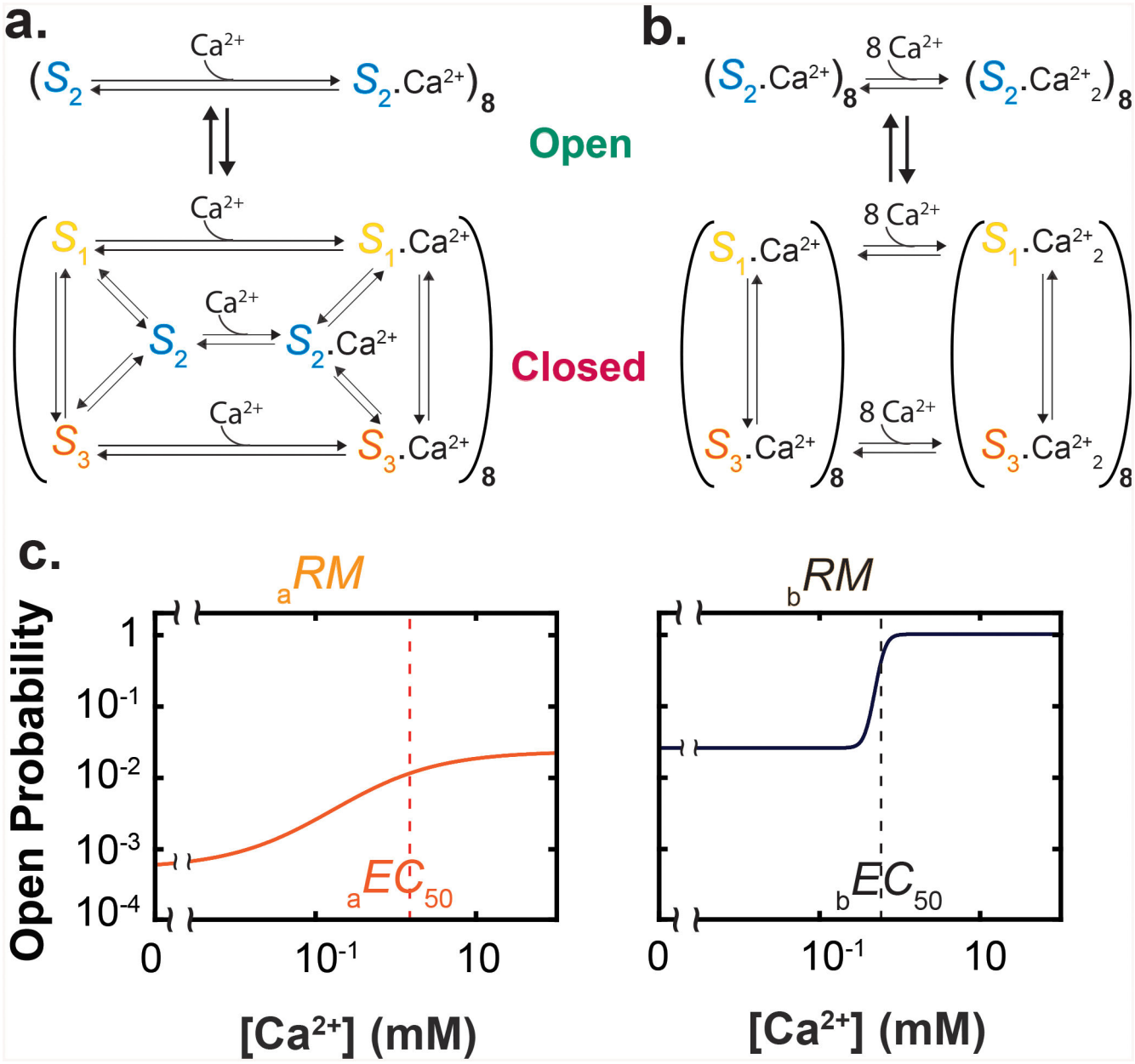

Figure 4.

Model of the regulatory module in two configurations. **a**. State diagram of $_{a}RM$ where in closed states, eight RCKs can independently adopt any of the three conformations, whereas in open states, all RCKs are in S_2, regardless of whether they are bound with Ca^{2+}. All-S_2 species with or without Ca^{2+} bound should be excluded from the closed state of the regulatory module in $_{a}RM$, but it was not explicitly done for graphic simplicity. **b**. State diagram of $_{b}RM$ where in closed states, individual RCKs can adopt S_1 or S_3 but not S_2, whereas in the open state, all RCKs are in S_2. **c**. Predicted open probabilities of $_{a}RM$ (orange, left) and $_{b}RM$ (black, right) plotted against the Ca^{2+} concentration. The vertical dashed lines indicate the EC_{50} value of the experimental p_o–$[Ca^{2+}]$ relation of the MthK channel[6].

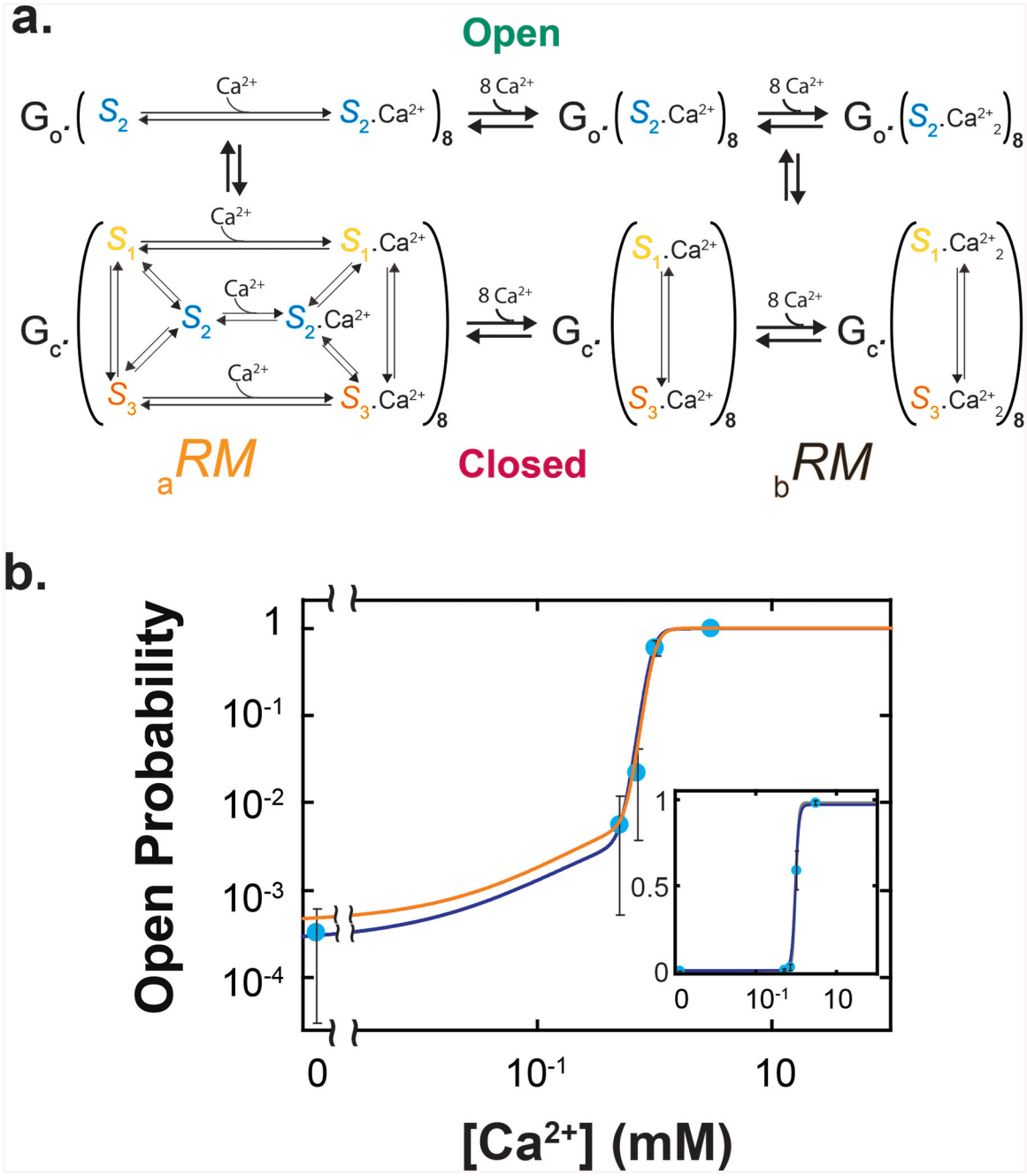

Figure 5.

Model for the whole MthK channel. **a**. State diagram of an energetic model for the whole channel. The gate (G) and the regulatory module (RM) both are either in an open state (o) or in a closed (c) state; RM can exist in $_{a}RM$ (left) or $_{b}RM$ (right). All-S_2 species with or without Ca^{2+} bound in $_{a}RM$ should be excluded from the closed state of the regulatory module, but it was not explicitly done for graphic simplicity. **b**. The calculated (orange) and fitted (blue) p_o–[Ca^{2+}] curves of the whole channel model (Eq. 15), plotted along the electrophysiological data previously obtained at pH 8.1 (mean ± s.e.m.)[6], where both p_o and the Ca^{2+} concentration are plotted on logarithmic scales; shown in the inset are the same

curves and data where p_o is plotted on a linear scale. The calculation and fit are performed as described in the text. The spontaneous $_{ch}p_o$ was estimated from a linear fit of the plot of observed $_{ch}p_o$ in the absence of Ca^{2+} versus pH[6].